Journal of Power Sources 196 (2011) 5209–5214

Contents lists available at ScienceDirect

Journal of Power Sources

journal homepage: www.elsevier.com/locate/jpowsour

Enhanced capacitance in partially exfoliated multi-walled carbon nanotubes

Gongming Wang[a], Yichuan Ling[a], Fang Qian[a], Xunyu Yang[a], Xiao-Xia Liu[b], Yat Li[a,*]

[a] Department of Chemistry and Biochemistry, University of California, 1156 High Street, Santa Cruz, CA 95064, USA
[b] Department of Chemistry, Northeastern University, Shenyang 110004, China

ARTICLE INFO

Article history:
Received 15 December 2010
Received in revised form 1 February 2011
Accepted 3 February 2011
Available online 12 February 2011

Keywords:
Supercapacitor
Exfoliated carbon nanotubes
Capacitance
Graphene
Multi-walled carbon nanotubes

ABSTRACT

We report for the first time the enhanced capacitance of multi-walled carbon nanotubes (MWCNTs) after exfoliation. Transmission electron microscopy studies confirmed that the MWCNTs were partially exfoliated with improved effective surface area. Carbon cloth electrode deposited with partially exfoliated carbon nanotubes (Ex-CNTs) yielded specific capacitances in a range of 130–165 F g^{-1} at charging/discharging current densities from 5 to 0.5 A g^{-1}, with coulombic efficiencies of ~98%. The specific capacitance of Ex-CNTs was an order of magnitude higher than untreated MWCNTs, and comparable to graphene at all charging/discharging current densities we studied. The enhanced capacitance can be attributed to improved effective surface area and increased defect density of the exfoliated tubular structure. The results declared that Ex-CNTs are promising electrode materials for high-capacitance supercapacitors.

Published by Elsevier B.V.

1. Introduction

Supercapacitors have recently been extensively investigated as energy storage devices because of their large specific energy and power density [1–11]. In comparison to conventional capacitors, supercapacitors have several orders of magnitude higher in specific energy density. Supercapacitors can also store and deliver a large amount of charge in a short period of time, which allows them deliver higher power than rechargeable batteries [12–14]. The capacitance of supercapacitor is built upon the formation of electrochemical double layer at the electrode/electrolyte interface, and thus, the active interfacial surface area is a key parameter that determines the capacitance [15–17]. One-dimensional (1D) carbon nanotubes (CNTs) are emerging as new electrode materials for supercapacitors, due to their high conductivity, high surface area range and good corrosion resistance [3,14,18]. The effective surface area of a supercapacitor material is referred to the active layer that is accessible by electrolyte ions [19], however, it is energetically unfavorable for solvated ions to diffuse into the inner tube of CNT [20], in particularly for multi-walled carbon nanotubes (MWCNTs). In this regard, the specific capacitance of MWCNTs, especially at high current operation, can be limited by the slow diffusion of ions. Although single-walled carbon nanotubes (SWCNT) have higher specific capacitance than MWCNT due to larger surface area per unit mass [1–3], the high cost of SWCNT limits their feasibility for device applications.

Considerable efforts have been placed to improve the specific capacitance of MWCNTs. For example, the CNTs treated with sulfuric acid or nitric acid showed several times enhanced capacitance due to the increased surface defect density, which facilitated the diffusion of ions into the inner tube [21,22]. Enhanced specific capacitance has also been observed in MWCNT based pseudocapacitors, where MWCNTs were decorated with metal oxides [23–27], and/or conducting polymer [28–32]. The enhanced capacitance in pseudocapacitors is due to faradaic type charge transfer instead of double layer electrostatic interaction. However, the charging/discharging cycling performance of pseudocapacitors can be limited by the irreversible redox reactions [33], and the possible structural changes of polymer appear in subsequent cycles [34]. The objective of this work is to develop a novel and simple way to enhance the capacitance of MWCNTs by increasing the active surface area and defect density through exfoliation.

2. Experimental methods

2.1. Materials

MWCNTs (95%) and graphite powder were purchased from Alfa Aesar. H_2SO_4 (98%), HCl (37%), HNO_3 68–70%, H_2O_2 (30%), hydrazine (64%) and $KMnO_4$ were obtained from Fisher Scientific Company. All chemicals were used as received, unless otherwise stated.

* Corresponding author. Tel.: +1 8314591952; fax: +1 8314592935.
E-mail address: yli@chemistry.ucsc.edu (Y. Li).

0378-7753/$ – see front matter. Published by Elsevier B.V.
doi:10.1016/j.jpowsour.2011.02.019

2.2. Preparation of Ex-CNTs

Ex-CNTs were prepared by a reported method with modest modification [35]. 0.25 g MWCNTs were dispersed into 15 ml concentrated H_2SO_4 and stirred for 1 h. Then 1.5 g $KMnO_4$ was added into the MWCNT solution at 50 °C. When all of the $KMnO_4$ were consumed, the reaction mixture was quenched by adding 40 ml deionized (DI) water and 3 ml 30% H_2O_2. The Ex-CNTs were extracted by centrifugation and washed with DI water.

2.3. Preparation of graphene

Graphite oxide was synthesized by a modified Hummers and Offenman's method from graphite powder [36–38]. 0.5 g graphite powder, 20 ml H_2SO_4 and 5 ml HNO_3 were mixed together in an ice bath. 3 g $KMnO_4$ was slowly added into the mixture, and heated the solution at 35 °C for 2 h. Then the solution was diluted by adding 140 ml DI water, followed by the slow addition of 3 ml H_2O_2. The aqueous graphite oxide solution was sonicated vigorously for 2 h to facilitate the separation of graphene oxide sheets. The graphene oxide precipitate was extracted, washed with DI water and then finally were reduced by hydrazine into graphene.

2.4. Preparation of electrodes

A carbon cloth was dipped into Ex-CNT containing aqueous solution, and then dried in an oven at 80 °C. The loading of Ex-CNTs can be controlled by repeating the dipping–drying process. Ex-CNTs were then reduced in hydrazine vapor at 60 °C from 2 to 144 h. Finally, the carbon cloth was washed with water to remove the loosely attached Ex-CNTs, and dried at 80 °C. The weight of completely dried carbon cloth was measured before and after the deposition of Ex-CNTs. All the samples for electrochemical measurements have the loading of about 1 mg cm^{-2}. Graphene and MWCNT electrodes were prepared by the similar method.

2.5. Methylene blue adsorption

18 mg of methylene blue (in excess) was dissolved in 400 ml ethanol solution, and then mixed with 5 mg of the analyte (Ex-CNTs or MWCNTs). The solution mixture was agitated for 12 h. The suspended particles were removed by centrifugation. 0.5 ml of the supernatant solution was collected and further diluted by a factor of 8 for UV–vis absorption spectroscopy. The amount of adsorbed methylene blue can be calculated based on the absorbance of the supernatant, by comparing it to the standard dilution curve of the methylene blue solution.

2.6. Brumauer–Emmett–Teller (BET) measurement

Nitrogen adsorption–desorption isotherms were measured with a Micromeritics Quadrasorb analyzer at 77 K. Before the measurements, the samples were degassed at 180 °C in vacuum for 6 h. The BET method was utilized to calculate the specific surface areas (S_{BET}) using adsorption data in a relative pressure range from 0.04 to 0.2. By using the Barrett–Joyner–Halanda model, the pore volumes (V_t) and pore size (D) distributions were derived from the adsorption branches of isotherms, and the total pore volumes were estimated from the adsorbed amount at a relative pressure P/P_0 of 0.992. The micropore volumes (V_{micro}) and micropore surface areas (S_{micro}) were calculated from the $V-t$ plot method using the equation $V_m/cm^3 = 0.001547 \times I$, where I represents the y intercept in the $V-t$ plots. The t values were calculated as a function of the relative pressure using the de Bore equation, $t/Å = [13.99/(\log(P_0/P) + 0.0340)]^{1/2}$.

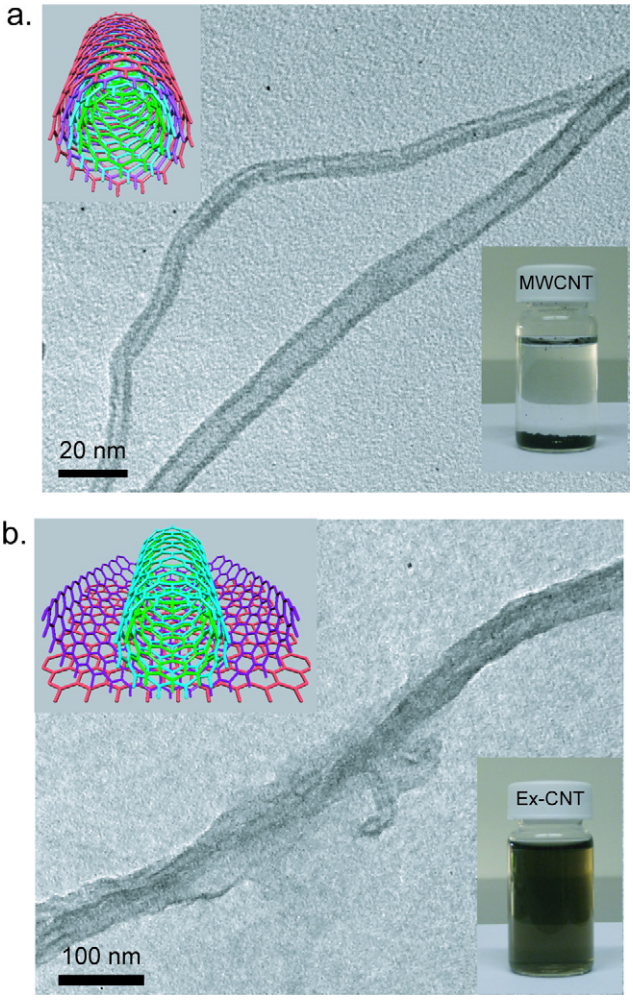

Fig. 1. Bright-field TEM images of (a) MWCNTs and (b) Ex-CNTs. Insets: pictures of MWCNTs and Ex-CNTs dispersed in aqueous solution, and the schematic diagrams of MWCNT and Ex-CNT.

2.7. Transmission electron microscopy (TEM) studies

Nanomaterials (CNTs, Ex-CNTs and graphene) were dispersed in aqueous solution and then transferred onto Cu/lacey carbon TEM grids. TEM images were collected in a JEOL 1200 EX TEM operated with a 120 kV electron beam.

2.8. Electrochemical measurements

Electrochemical studies were carried out in a three-electrode cell with nanomaterial coated carbon cloth as working electrode, Pt wire as counter electrode and an Ag/AgCl electrode as a reference. Electrolyte was a 3 M NaOH aqueous solution. Electrochemical properties were measured by an electrochemical workstation (CHI 660D).

3. Results and discussion

Ex-CNTs were prepared by a reported method with modest modification [35]. TEM analysis was carried out on MWCNTs before and after the oxidation. TEM image showed that the untreated MWCNTs have tubular structures with smooth surface (Fig. 1a). Significantly, the surface of tubular MWCNTs became blurry after 3-h oxidation treatment (Fig. 1b). Additional TEM images of Ex-CNTs are illustrated in Fig. S1, Supporting Information. These results

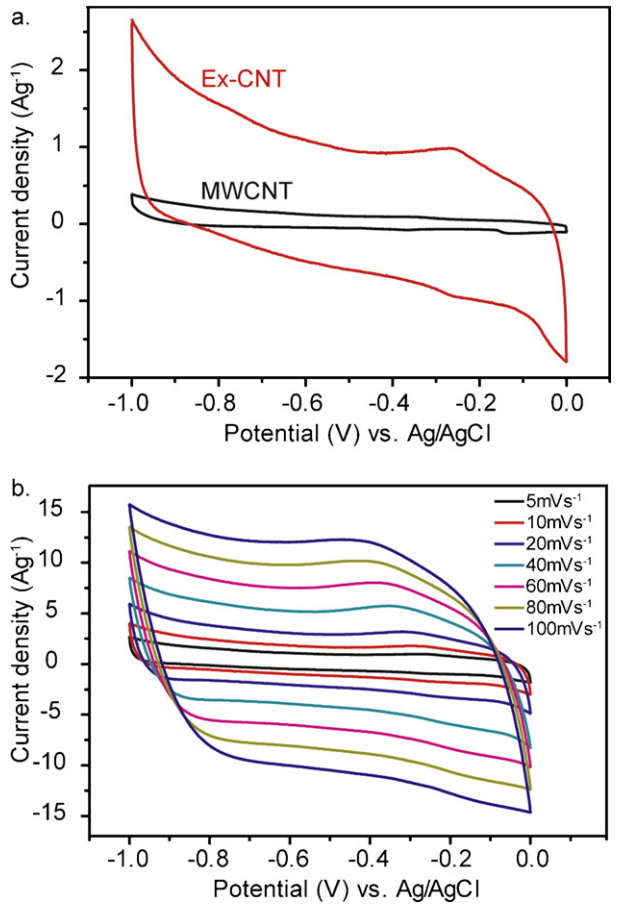

Fig. 2. Cyclic voltammograms collected from (a) Ex-CNT and MWCNT electrodes at a scan rate of 5 mV s^{-1} and (b) the Ex-CNT electrode at scan rates from 5 to 100 mV s^{-1}.

suggested the MWCNTs were partially exfoliated (Fig. 1b, inset). Moreover, the MWCNTs showed substantially enhanced water solubility after exfoliation/oxidation (Fig. 1a, inset), as a result of the attachment of oxygen-containing groups (*e.g.*, –C–OH, –C=O) on the tube surface. Importantly, it allows Ex-CNTs to be easily assembled on different hydrophilic substrates, including the flexible substrates such as carbon cloth or cotton cloth. In this work, we employed carbon cloth as electrode. In comparison to conventional metal electrode, carbon cloth is flexible, lightweight, low-cost and offers large surface area for active material loading. Ex-CNTs can be well entangled with the fibers of carbon cloth and expected to have low contact resistance.

Ex-CNT-coated carbon cloth electrodes were characterized by cyclic voltammetry (CV) and galvanostatic charging/discharging measurements in a three-electrode electrochemical cell with 3 M NaOH solution as electrolyte. MWCNT-coated carbon cloth electrodes prepared under similar conditions were measured for comparison. Fig. 2a compared the CVs of MWCNT and Ex-CNT samples collected at a scan rate of 5 mV s^{-1}. The capacitance of the blank carbon cloth is negligible (Fig. S2, Supporting Information). Because the specific capacitance is proportional to the area of CV curve, the results clearly showed that Ex-CNTs have substantially higher specific capacitance than MWCNTs. In addition, a small redox pair was observed on the CV curve of Ex-CNTs at −0.26 V (Fig. 2a), suggesting combined capacitance of pseudocapacitance and double layer capacitance for Ex-CNTs. The observed pseudocapacitance can be due to the presence of oxygen-containing groups on Ex-CNTs as a result of incomplete chemical reduction. All CV curves of Ex-CNTs collected at various scan rates up to 100 mV s^{-1} (Fig. 2b) displayed similar slightly distorted rectangular shapes, suggesting a high power density for Ex-CNTs. These data indicate efficient charge accumulation and ion diffusion at the interface between Ex-CNT electrode and electrolyte, which is especially critical for device operation at high charging/discharging current density. Ex-CNT based electrode could potentially address capacitance degradation at high charging/discharging current density that has been a limitation for commercialized activated carbon supercapacitors [39].

The specific capacitances of Ex-CNT- and MWCNT-coated electrodes were characterized by galvanostatic charging/discharging measurements. Galvanostatic cycling data obtained from the Ex-CNT at a charging/discharging current density of 1 A g^{-1} showed linear discharging curves in the potential range with a nearly constant slope, indicating excellent capacitive behavior of Ex-CNTs (Fig. 3a) [40,41]. The time required for a single charging–discharging cycle for Ex-CNT and MWCNT electrodes were compared in Fig. 3b. It takes substantially longer time to charge Ex-CNT electrode than that of MWCNT at the same current density of 1 A g^{-1}, again confirming larger capacitance of Ex-CNT (Fig. 3b). The specific capacitances of the electrodes were calculated using the following equation:

$$\text{specific capacitance} = \frac{i \times t}{V \times m} = \frac{i}{S \times m}$$

where S is the slope of discharging curve (V s^{-1}), i is charging/discharging current, m is weight of the active material (the weight of carbon cloth is not included because of its negligible capacitance) and therefore i/m is the charging/discharging current per unit mass (A g^{-1}). The calculated specific capacitances of Ex-CNT and MWCNT at the charging/discharging current density of 1 A g^{-1} were 154.4 F g^{-1} and 11.8 F g^{-1}, respectively. The specific capacitance of MWCNT is comparable to the best literature reported values [18,42,43]. Significantly, Ex-CNTs showed an order of magnitude enhanced capacitance compared to MWCNTs. The improved capacitance can be attributed to the improved effective surface area per unit mass of Ex-CNTs as well as the increased defect density.

To confirm the increase of effective surface area in Ex-CNTs compared to MWCNTs, both methylene blue as well as BET adsorption measurements were performed on the samples. Methylene blue adsorption has been used as an indicator of graphitic material surface areas in previous studies, in which each milligram of adsorbed methylene blue represents 2.45 m^2 of surface area [44–46]. A fixed amount of analyte (Ex-CNTs or MWCNTs) was mixed with excess methylene blue solution of known concentration. By determining methylene blue concentration after the reaction using UV–vis spectroscopy (see Section 2), the amount of adsorbed methylene blue and thereby the surface area of analyte can be calculated. The surface area of MWCNT and Ex-CNT were calculated to be ~280 and 480 m^2 g^{-1}, respectively, suggesting the effective surface area of MWCNTs was enhanced after oxidation. However, the fact that the surface topology and chemistry of material may influence the area occupied by each methylene blue molecule and cause possible inaccuracy in determining material surface area, BET surface adsorption measurements were also performed on the samples for comparison (see Section 2). The BET adsorption data are summarized in Table 1. Significantly, Ex-CNTs sample showed more than two times enhancement in specific surface area (391 m^2 g^{-1}) compared to untreated MWCNTs (172 m^2 g^{-1}), which is consistent with the methylene blue adsorption results. In addition, Ex-CNTs have larger pore volume that is expected to be favorable for solvated ion diffusion. Taken together, these results clearly confirmed the surface area enhancement in MWCNT after oxidation, and served as a strong evidence for successful exfoliation of MWCNT.

Moreover, the increased defect density during exfoliation process could also facilitate the diffusion of solvated ions into inner tube, as reported previously [47]. The defect densities of MWCNT and Ex-CNT samples were characterized by Raman spectroscopy

Table 1
Summary of BET adsorption data for MWCNT, Ex-CNT and graphene.

	S_{BET} ($m^2\,g^{-1}$)	S_{micro} ($m^2\,g^{-1}$)	V_t ($cm^3\,g^{-1}$)	V_{micro} ($cm^3\,g^{-1}$)	D (nm)
Ex-CNT	391	116	0.670	0.051	2.2
MWCNT	172	61	0.581	0.026	2.9
Graphene	464	115	0.479	0.052	2.3

S_{BET} is the BET total surface area; S_{micro} is the mircopore surface area; V_t is the total pore volume; V_{micro} is the micropore volume; D is the mesopore size diameter.

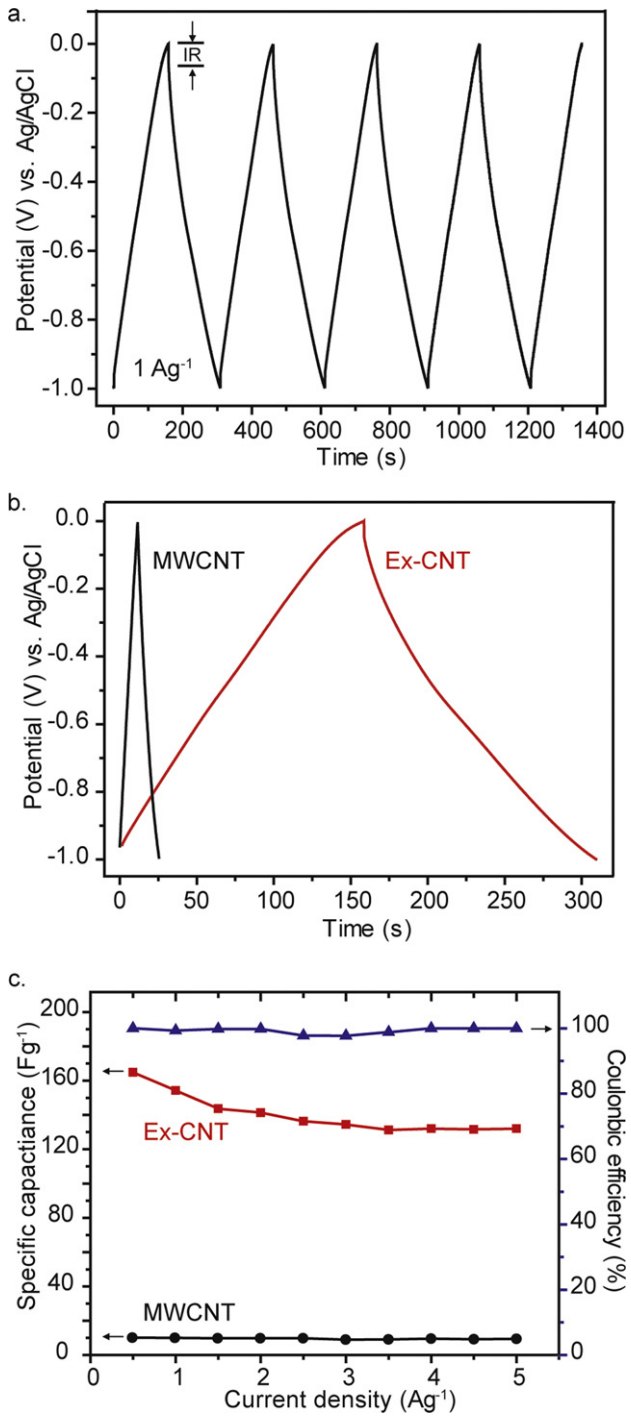

Fig. 3. (a) Galvanostatic cycling data of Ex-CNT electrode at charging/discharging current density of $1\,A\,g^{-1}$. (b) Comparison of galvanostatic curves of MWCNTs and Ex-CNTs in a single charging/discharging cycle at $1\,A\,g^{-1}$. (c) Calculated specific capacitance and coulombic efficiency of Ex-CNTs at different charging/discharging current densities; calculated specific capacitance of MWCNTs is plotted for comparison.

(Fig. S3, Supporting Information), which is a powerful approach to investigating the structural and electronic properties of carbon-based materials. It has been reported that D band of carbon material is defect dependent, and the intensity ratio of G band to D band is a good indication for the density of defects present in the materials (the higher the ratio, the less the defect density) [48,49]. Raman data (Fig. S3, Supporting Information) showed that the ratio decreases from 0.98 to 0.87 after exfoliation, confirming the increased defect density in Ex-CNT.

The capacitances of Ex-CNT based electrodes were measured at different charging/discharging current densities from 0.5 to $5\,A\,g^{-1}$ (Fig. 3c). The Ex-CNT exhibited a maximal specific capacitance of $165\,F\,g^{-1}$ at charging current density of $0.5\,A\,g^{-1}$, and slightly reduced to $133\,F\,g^{-1}$ at a larger charging current density of $5\,A\,g^{-1}$. The large specific capacitances at $5\,A\,g^{-1}$ together with the observed nearly rectangular CV curves at a high scan rate of $100\,mV\,s^{-1}$ (Fig. 2b) confirmed the excellent ion accessibility

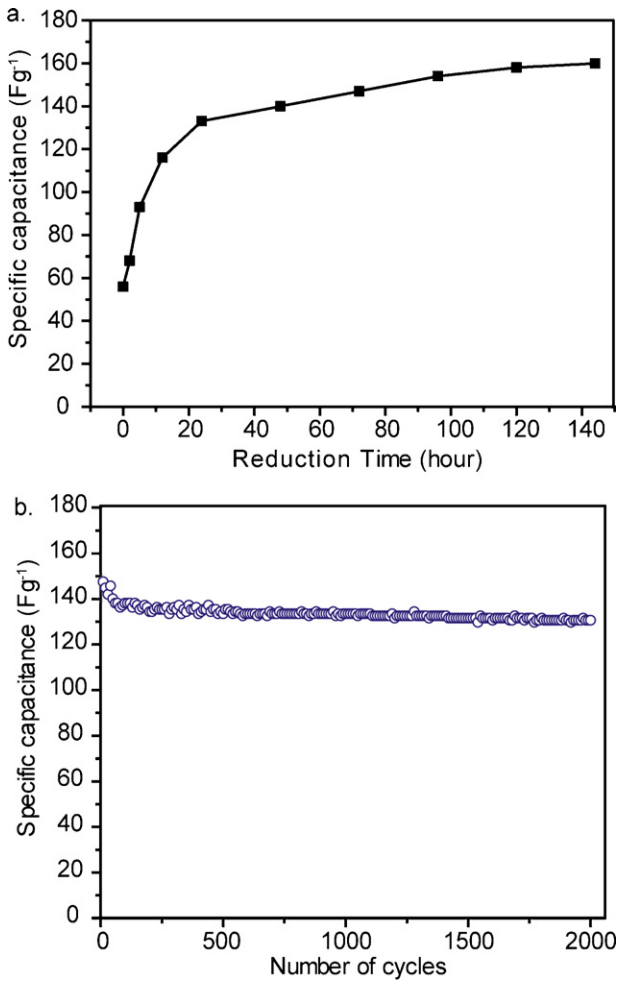

Fig. 4. (a) The specific capacitance of Ex-CNT electrode prepared under different reduction times. (b) The specific capacitance of Ex-CNTs is plotted as a function of galvanostatic charging/discharging cycles with a current density of $1\,A\,g^{-1}$.

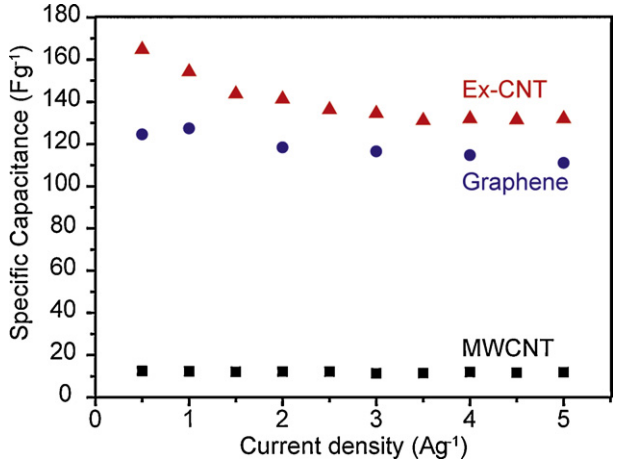

Fig. 5. Comparison of specific capacitance of MWCNTs, graphene and Ex-CNTs obtained at charging/discharging current densities from 0.5 to 5 A g^{-1}.

between Ex-CNT and electrolyte. To determine the reversibility of charging–discharging processes, we measured the coulombic efficiency (CE) of the electrodes, which is defined by the equation [7]:

$$CE = \frac{t_{discharging}}{t_{charging}}$$

where $t_{discharging}$ and $t_{charging}$ are discharging and charging time. The CE of Ex-CNTs is above 98% in the whole current density range from 0.5 to 5 A g^{-1} (Fig. 3c), indicating the charging–discharging processes were highly reversible.

Electrical conductivity of electrode material is another critical parameter that determines the capacitive performance. As-prepared Ex-CNTs have low electrical conductivity due to oxidization during the exfoliation process [35]. Therefore, the Ex-CNTs were further reduced in hydrazine vapor to increase the conductivity prior to electrochemical measurements. Their specific capacitances were studied as a function of reduction time. As shown in Fig. 4a, the specific capacitance increases drastically with reduction time because the improved electrical conductivity as a result of decrease of oxygen-containing groups on Ex-CNT. The prolonged reduction process only slightly improved the specific capacitance, indicating most of the oxidized Ex-CNTs have been reduced in the first 24 h. By optimizing the reduction time, Ex-CNT electrode yielded a maximal specific capacitance of 160 F g^{-1} at the charging/discharging current density of 1 A g^{-1}, which is comparable to the best reported values of carbon-based supercapacitors at the same current density [1,2,11]. Galvanostatic cycling studies on Ex-CNT electrodes at 1 A g^{-1} showed that the specific capacitance dropped quickly from 147 F g^{-1} to 138 F g^{-1} in the first 100 charging/discharging cycles, and then became stable with minor reduction of specific capacitance (138–130 F g^{-1}) in the following 1900 cycles (Fig. 4b). Overall, the Ex-CNT electrode showed good cycling stability, with a ~11% reduction of specific capacitance after 2000 charging/discharging cycles. These results revealed Ex-CNTs are efficient and stable electrode material for supercapacitors.

Finally, the capacitive performance of Ex-CNTs was compared to graphene, which has been used as electrodes for different energy storage devices [4,5,50]. TEM image shows that the as-prepared graphene oxide has a very thin 2D structure (Fig. S4, Supporting Information). These non-conducting graphene oxide materials were coated on carbon cloth and then reduced in hydrazine vapor into graphene for CV and galvanostatic cycling studies. The CV of graphene-coated electrode collected at different scan rates from 5 to 100 mV s^{-1} showed highly distorted rectangular shapes at high scan rates (Fig. S5, Supporting Information), which suggested the diffusion of electrolyte ions in graphene is less efficient compared to that in Ex-CNTs. The limited ion diffusion could be ascribed to the aggregation of graphene sheets during the reduction process and storage, as a result of the strong face-to-face attraction between graphene layers. The graphene sheets located inside the aggregate may not be accessible by the solvated ions that could significantly reduce the effective surface area [4,38,51]. BET adsorption data obtained from graphene and Ex-CNT samples (Table 1) shows that the surface area per unit mass of Ex-CNTs is slightly smaller than that of graphene, as expected. On the other hand, Ex-CNTs have larger total pore volume that is more favorable for solvated ion diffusion compared to graphene, which is in agree with the CV data. Fig. 5 compared the capacitive performance of MWCNT, graphene and Ex-CNT. Based on the galvanostatic measurements, the maximal specific capacitance of graphene-coated electrode was calculated to be about 127 F g^{-1} at charging/discharging current density of 1 A g^{-1}, which is comparable to the best literature reported data for graphene based supercapacitors [4,5]. Significantly, Ex-CNTs has comparable, if not better, specific capacitance with graphene sample at all charging/discharging current densities we studied.

4. Conclusions

We have successfully synthesized the partially exfoliated MWCNTs and studied the capacitive performance of these Ex-CNTs-coated electrodes. They exhibited a maximal specific capacitance of 165 F g^{-1} at a charging/discharging current density of 0.5 A g^{-1}, and a coulombic efficiency of ~98%. Significantly, the specific capacitances of Ex-CNTs are an order of magnitude higher than untreated MWCNT, and comparable to graphene at all charging/discharging current densities we studied. The enhanced capacitance is attributed to the increased effective surface area and defect density in the partially exfoliated tubular structure. Ex-CNTs hold great promise as electrode material for supercapacitors, and can possibly be used in other applications such as lithium ion batteries.

Acknowledgements

Y.L. acknowledges the support of this work by UCSC new faculty start up fund and NSF CAREER award (DMR-0847786). X.X.L. thanks the financial support from National Natural Science Foundation of China (project number 50973013).

Appendix A. Supplementary data

Supplementary data associated with this article can be found, in the online version, at doi:10.1016/j.jpowsour.2011.02.019.

References

[1] L. Hu, J.W. Choi, Y. Yang, S. Jeong, F.L. Mantia, L. Cui, Y. Cui, Proc. Natl. Acad. Sci. U.S.A. 106 (2009) 21490–21494.
[2] L. Hu, M. Pasta, F.L. Mantia, L. Cui, S. Jeong, H.D. Deshazer, J.W. Choi, S.M. Han, Y. Cui, Nano Lett. 10 (2010) 708–714.
[3] M. Kaempgen, C.K. Chan, J. Ma, Y. Cui, G. Gruner, Nano Lett. 9 (2009) 1872–1876.
[4] M.D. Stoller, S.J. Park, Y. Zhu, J. An, R.S. Ruoff, Nano Lett. 8 (2008) 3498–3502.
[5] Y. Wang, Z. Shi, Y. Huang, Y. Ma, C. Wang, M. Chen, Y. Chen, J. Phys. Chem. C 113 (2009) 13103–13107.
[6] C. Yu, C. Masarapu, J. Rong, B. Wei, H. Jiang, Adv. Mater. 21 (2009) 4793–4797.
[7] L. Chen, L.J. Sun, F. Luan, Y. Liang, Y. Li, X.X. Liu, J. Power Sources 145 (2010) 3742–3747.
[8] H. Wang, H.S. Casalongue, Y. Liang, H. Dai, J. Am. Chem. Soc. 132 (2010) 7472–7477.
[9] C. Liu, Z. Yu, D. Neff, A. Zhamu, B.Z. Jang, Nano Lett. 10 (2010) 4863–4868.
[10] M. Wu, M. Wang, Chem. Commun. 46 (2010) 6968–6970.
[11] K. Zhang, L.L. Zhang, X.S. Zhao, J. Wu, Chem. Mater. 22 (2010) 1392–1401.

[12] M. Winter, R.J. Brodd, Chem. Rev. 104 (2004) 4245–4270.
[13] A. Burke, J. Power Sources 91 (2000) 37–50.
[14] A.G. Pandolfo, A.F. Hollenkamp, J. Power Sources 157 (2006) 11–27.
[15] J. Chmiola, G. Yushin, Y. Gogotsi, C. Portet, P. Simon, P.L. Taberna, Science 313 (2006) 1760–1763.
[16] E. Frackowiak, F. Beguin, Carbon 39 (2001) 937–950.
[17] J. Gamby, P.L. Taberna, P. Simon, J.F. Fauvarques, M. Chesneau, J. Power Sources 101 (2001) 109–116.
[18] S. Talapatra, S. Kar, S.K. Pal, R. Vajtai, L. Ci, P. Victor, M.M. Shaijumon, S. Kaur, O. Nalamasu, P.M. Ajayan, Nat. Nanotech. 1 (2006) 112–116.
[19] A.L.M. Reddy, S. Ramaprabhu, J. Phys. Chem. C 111 (2007) 7727–7734.
[20] H. Shimoda, B. Gao, X.P. Tang, A. Kleinhammes, L. Fleming, Y. Wu, O. Zhou, Phys. Rev. Lett. 88 (2002) 015502.
[21] C.G. Liu, H.T. Fang, F. Li, M. Liu, H.M. Chen, J. Power Sources 160 (2006) 758–761.
[22] K. Jurewicz, K. Babel, R. Pietrzak, S. Delpeux, H. Wachowska, Carbon 44 (2006) 2368–2375.
[23] R.R. Bi, X.L. Wu, F.F. Cao, L.Y. Jiang, Y.G. Guo, L.J. Wang, J. Phys. Chem. C 114 (2010) 2448–2451.
[24] X. Xie, L. Gao, Carbon 45 (2007) 2365–2373.
[25] A.K. Mishra, S. Ramaprabhu, J. Phys. Chem. C 114 (2010) 2583–2590.
[26] X. Du, C. Wang, M. Chen, Y. Jiao, J. Wang, J. Phys. Chem. C 113 (2009) 2643–2646.
[27] A. Reddy, M.M. Shaijumon, S.R. Gowda, P.M. Ajayan, J. Phys. Chem. C 114 (2010) 658–663.
[28] M. Wu, L. Zhang, D. Wang, J. Gao, S. Zhang, Nanotechnology 18 (2007) 385603.
[29] Y. Hou, Y. Cheng, T. Hobson, J. Liu, Nano Lett. 10 (2010) 2727–2733.
[30] Y. Fang, J. Liu, D.J. Yu, J.P. Wicksted, K. Kalkan, C.O. Topal, B.N. Flanders, J. Wu, J. Li, J. Power Sources 195 (2010) 674–679.
[31] Q. Li, J. Liu, J. Zou, A. Chunder, Y. Chen, L. Zhai, J. Power Sources 196 (2010) 565–572.
[32] A. Snook, P. Kao, A.S. Best, J. Power Sources 196 (2010) 1–12.
[33] E. Raymundo-Pinero, V. Khomenko, E. Frackowiak, F. Beguin, J. Electrochem. Soc. 152 (2005) A229–A235.
[34] L. Li, H. Song, Q. Zhang, J. Yao, X. Chen, J. Power Sources 187 (2009) 268–274.
[35] D.V. Kosynkin, A.L. Higginbotham, A. Sinitskii, J.R. Lomeda, A. Dimiev, B.K. Price, J.M. Tour, Nature 458 (2009) 872–876.
[36] W.S. Hummers, R.E. Offeman, J. Am. Chem. Soc. 80 (1958) 1339.
[37] S. Gilje, S. Han, M. Wang, K.L. Wang, R.B. Kaner, Nano Lett. 7 (2007) 3394–3398.
[38] L.J. Cote, F. Kim, J. Huang, J. Am. Chem. Soc. 131 (2009) 1043–1049.
[39] D. Hulicova, J. Yamashita, Y. Sooneda, H. Hatori, M. Kodama, Chem. Mater. 17 (2005) 1241–1247.
[40] D.Y. Qu, J. Power Sources 109 (2002) 403–411.
[41] A.J. Burke, J. Power Sources 91 (2000) 37–50.
[42] A.K. Cuentas-Gallegos, R. Martinez-Rosales, M. Baibarac, P. Gomez-Romero, M.E. Rincon, Electrochem. Commun. 9 (2007) 2088–2092.
[43] G.P. Pandey, S.A. Hashmi, Y. Kumar, J. Electrochem. Soc. 157 (2010) A105–114.
[44] C.S. Hannes, J. Li, M.J. McAlister, S. Hiroaki, M. Herrera-Alonso, D.H. Adamson, R.K. Prud'homme, R. Car, D.A. Saville, I.A. Aksay, J. Phys. Chem. B 110 (2006) 8535–8539.
[45] M.J. McAlister, J. Li, D.H. Adamson, H.C. Schniepp, A.A. Abdala, J. Liu, M. Herrera-Alonso, D.L. Milius, R. Car, R.K. Prud'homme, I.A. Aksay, Chem. Mater. 19 (2007) 4396–4404.
[46] H. Kim, A.A. Abdala, C.W. Macosko, Macromolecules 43 (2010) 6515–6530.
[47] C. Liu, H. Cao, P.Y. Li, H. Xu, Y. Zhang, Carbon 44 (2006) 2919–2924.
[48] L. Jiao, L. Zhang, X. Wang, G. Diankov, H. Dai, Nature 458 (2009) 877–880.
[49] S. Costa, B. Scheibe, M. Rummeli, E. Borowiak-Palen, Phys. Status Solidi. 246 (2009) 2717–2720.
[50] D. Wang, F. Li, J. Zhao, W. Ren, Z. Chen, J. Tan, Z. Wu, I. Gentle, G.Q. Lu, H. Cheng, ACS Nano 3 (2009) 1745–1752.
[51] S. Stankovich, D.A. Dikin, R.D. Piner, K.A. Kohlhass, A. Kleinhammes, Y. Jia, Y. Wu, S.T. Nguyen, R.S. Ruoff, Carbon 45 (2007) 1558–1565.